Eur. Phys. J. B **41**, 135–145 (2004)
DOI: 10.1140/epjb/e2004-00302-y

THE EUROPEAN PHYSICAL JOURNAL B

Stability of oscillatory flows past compliant surfaces

R.M. Thaokar and V. Kumaran[a]

Department of Chemical Engineering Indian Institute of Science Bangalore 560 012, India

Received 19 December 2003 / Received in final form 17 March 2004
Published online 30 September 2004 –

Abstract. The stability of oscillatory flows over compliant surfaces is studied analytically and numerically. The types of compliant surfaces studied are the spring backed wall model, which permits tangential motion of the surface, and the incompressible viscoelastic gel model. The stability is determined using the Floquet analysis, where amplitude of perturbations at time intervals separated by one time period is examined to determine whether perturbations grow or decay. The oscillatory flows past both the spring backed wall model and the viscoelastic gel model exhibit an instability in the limit of zero Reynolds number, and the transition amplitude of the oscillatory velocity increases with the frequency of oscillations. The transition amplitude has a minimum at zero wave number for the spring backed plate model, whereas the minimum occurs at finite wavenumber for the viscoelastic gel model. For the spring backed plate model, it is shown that the instability due to steady mean flow and the purely oscillatory instability reinforce each other, and the regions of instability are mapped in the $(\Lambda - A)$ plane, where Λ is the steady strain rate and A is the oscillatory strain rate. For the viscoelastic gel model, the instability is found to depend strongly on the gel viscosity η_g, and the effect of oscillations on the continuation of viscous modes at intermediate Reynolds number shows a complicated dependence on the oscillation frequency.

PACS. 47.20.Ft Instability of shear flows – 83.50.-v Deformation and flow – 87.19.Tt Rheology of body fluids

1 Introduction

Fluid flow over soft materials is ubiquitous in biological as well as in technological applications. These soft materials could be infinitesimally thin viscoelastic membranes, like those occurring in red blood cells, or flexible walls of finite thickness, like the walls of blood vessels. The dynamics of fluid flow past flexible surfaces is qualitatively different from the flow over rigid surfaces, because of the coupling between the fluid and the wall dynamics, and the wall properties can influence the stability characteristics in a non-trivial manner. Oscillatory flow over soft materials are encountered in the flow of cardiovascular fluids through flexible blood vessels which are driven by the pumping of the heart. The Reynolds numbers for these flows varies over a wide range between $Re < 1$ and $Re = 4000$ [1]. The oscillatory nature of the blood flow in the vascular system is characterized by a number often called the Womersley or Witzig number $\alpha = R\sqrt{(\omega/\nu)}$, where R is the artery diameter, ω is the oscillatory frequency and ν is the kinematic viscosity of the cardiovascular fluid, and these arterial flows can be affected by the wall elasticity and conditions like stenosis, when the arteries get narrowed and obstructed. There has been great deal of experimental and computational fluid dynamics studies to calculate the oscillatory and peristaltic fluid flow through elastic tubes. The elasticity of the wall is carefully accounted for in the analysis, and is found to affect the flow in a significant manner. However, all these studies are carried out for fluid flow through tubes or surfaces which, although flexible, are of fixed geometries. Not much work has been done on the moving boundary elastic solid-fluid interaction problems, and so the problem of onset of instability and full numerical evolution of perturbations has not been addressed till date.

The objective of the study of the stability of steady flows is to determine whether the growth rate of perturbations in time is positive or negative. It is difficult to use a similar procedure for oscillatory flows, since the mean velocity is a periodic function of time. If the growth rate is large compared to the frequency of oscillations, it is possible to approximate the flow at any instant of time as a steady flow with the instantaneous mean velocity, and examine the growth of perturbations for this flow. In this case, it is expected that if the velocity at any point in the oscillatory cycle is greater than the critical velocity for the steady flow, perturbations will grow rapidly in a time scale short compared to the period of oscillation and take the system into the non-linear regime. However, if the growth rate is not large compared to the frequency of

[a] e-mail: kumaran@chemeng.iisc.ernet.in

oscillations, the growth of perturbations during the part of the cycle when the velocity is greater than the critical velocity for a steady flow could be compensated by the decay of perturbations during the part of the cycle when the velocity is lower than that for a steady flow. In this case, it is necessary to examine the relative amplitude of perturbations at equal phase angles in successive cycles, in order to determine whether there is growth or decay of perturbations as the cycles progress. This is carried out in the present study using the Floquet analysis.

The stability of a horizontal liquid layer on an oscillating plate was studied by Yih [2] using low wavenumber asymptotic analysis. The oscillatory flow was shown to be unstable, although the non-oscillatory flow is stable. Von Kerckzek and Davis [3] studied the flow of a layer of fluid down an inclined oscillating plane. This system is known to be unstable in the absence of oscillation, and Von Kerckzek and Davis [3] calculated the stability windows for this flow in the presence of oscillations. This analysis indicates that although the Stokes layer has velocity profiles with inflection points, those are unstable only at low frequencies. At sufficiently high frequencies, the inflectional unstable modes may not have enough time to grow, and can be eventually stabilized by the rapidly oscillating flow. Coward and Papageorgiou [4] studied the stability of two-phase Couette flow bounded between plane parallel plates using the long wave analysis of Yih [2], where one of the bounded plates had a time dependent velocity in its plane. The time dependent velocity had a constant and an oscillatory time periodic part. The flow is unstable in the nonoscillatory regime due to an interfacial instability if the viscosities are different. Using Floquet theory, the authors showed that in the long wave limit, the time modulations can have significant influence on flow stability. Their analysis showed that flows which are otherwise unstable can be stabilized by oscillations. King et al. [5] studied the problem of oscillatory two-phase Couette flow experimentally as well as numerically. Since the Floquet theory gives only time averaged growth rates, they calculated the transient instability numerically and showed that the interfacial wave amplification actually originates with an internal disturbance, and is not directly caused by interfacial shear. Coward and Renardy [6] studied the effect of oscillatory forcing as a dynamic stabilisation mechanism for two-layer plane Couette-Poiseuille flow at low Reynolds numbers using numerical and asymptotic methods. They found that the oscillations can have stabilising or destabilizing effect depending upon the conditions of the flow. Complete stabilisation is possible for certain flows which are otherwise unstable owing to the viscosity stratification across the interface. The combined pressure and velocity fluctuations can have an effect on the flow stability opposite to that induced by the time-periodic forcing mechanisms. There has been very little work on the stability of viscoelastic oscillatory flows. Ramaan et al. [7] studied the stability of viscoelastic shear flows subjected to steady and oscillatory transverse flows. Their study showed that superposition of axial periodic motion on circular Couette and Dean flows can delay the onset of the viscoelastic instability. However, there does not seem to have been much work done on the stability of oscillatory fluid flows over compliant surfaces, which forms the basis of the present work.

There have been a large number of studies, motivated by drag reduction in marine and aerospace applications [8–12], of the steady flow of a Newtonian fluid past a flexible surface. These have modeled the flexible wall to be a thin spring-backed plate membrane. The high Reynolds number Tollmien – Schlichting instability (TSI) is modified owing to the flexibility of the wall. Benjamin [13] extended the classical stability theory of Tollmien and Schlichting (see, for example, Drazin and Reid [14]) and showed that a flexible non-dissipative wall tends to stabilise the TSI, which is the destabilising mechanism in flow past rigid surfaces. In addition, Benjamin [15] and Landahl [16] pointed out that there is an additional mode of instability that could exist in an inviscid flow, which was termed the 'flow-induced surface instability' (FISI). Carpenter and Garrad [11,12] analysed the stability of Blasius flow over a compliant plate, in which they considered both TSI and FISI. The TSI was analysed numerically, while FISI was analysed using both analytical and numerical methods. These studies concluded that the wall flexibility usually stabilises the flow in the boundary layer and increases the Reynolds number at which transition to turbulence occurs. Carpenter and Morris [10] analysed the effect of anisotropic wall compliance on the stability of Blasius boundary layer flow past flexible surface modelled as a spring-backed wall. Unlike the earlier studies of Carpenter and co-workers, this study included both normal and tangential motion in the plate-membrane wall. Davies and Carpenter [8] studied the stability of the plane-Poiseuille flow in a compliant channel. This study modelled the compliant walls as spring-backed plates with only normal wall motion. This study analysed the interconnected behaviour of FISI and TSI using both asymptotic and numerical methods, and found that if the compliant wall properties are selected to give a significant stabilising effect on TSI, the onset of FISI could be severely affected.

Another model that has been used for the flexible wall is the continuum visco-elastic wall model [17–22]. In this case, the wall material is modeled as a visco-elastic continuum, and the dynamical description is based on the displacement field, which provides the displacement of material points from their equilibrium positions due to stresses exerted on the wall. There is an elastic stress due to the strain in the material, and a viscous stress due to the strain rate. The theoretical results [17] for the viscous instability were found to be in agreement with the experimental results [21] with no adjustable parameters. In the present analysis, we consider the stability of oscillatory flows past compliant walls of the spring-backed membrane type and the continuum visco-elastic type.

Oscillatory flows are unsteady, and it is important to precisely define the stability of an unsteady flow. Presented below is the description of stability in unsteady flows as discussed in Davis [23]. In oscillatory flows, since the basic state itself is unsteady, a natural measure of the system stability would be the comparison between

the growth rate of the system and the rate of change of the base state. However difficulties arise in interpretation, since the time periodic base state accelerates in the first cycle and decelerates in the second half. A system would be called monotonically stable if the disturbances decay at every point in time. However there can be cases in which the disturbances grow in the first half of the cycle and then decay, so that there is a net decay of the perturbation over the cycle. These are called transiently stable systems. However, the perturbation can attain sufficient amplitude during the growth cycle, so that the perturbation amplitude is no longer small compared to the mean flow velocity. In this case, nonlinear interactions can then lead to secondary flows. This is a more difficult mathematical problem, and in the present analysis, we assume that the amplitude of the disturbances remain small at all times over the cycle, so that the non-linear terms can be neglected.

Oscillatory systems are characterised by an additional time scale in the system, the oscillation frequency, which also gives an additional length scale, called the Stokes length $(\nu/\omega)^{1/2}$. The perturbations due to plate oscillations result in velocity disturbances over length scales comparable to the Stokes length. When the Stokes length is small compared to the width of the channel, the flow resembles a boundary layer flow where disturbances are localized near the oscillating plate, and it is expected that interfacial instabilities will not be affected by this type of forcing. The most interesting regime is when the Stokes length is comparable to the width of the channel, when there is a coupling between the motion of the top plate and the interfacial motion. This regime is examined in the present analysis.

The article is organised as follow. The Floquet theory of dynamical equations is discussed in Section 2. The instability in oscillatory flow over spring backed plates in discussed in Section 3, and the oscillatory flow instability over viscoelastic gels is analysed in Section 4. The experimental results for the low Reynolds number instability in flow over viscoelastic gels is presented in Section 5.

2 Floquet theory for the dynamical equations

The Floquet analysis is used to determine the stability of time periodic base states or limit cycles. A Floquet exponent larger than one implies that the limit cycle is unstable to small perturbations. The relation between the Floquet exponents and the characteristic root, which is the growth rate in the linear analysis for a non-oscillatory flow, is as follows. Consider a linear dynamical system governed by the equation

$$\dot{\mathbf{x}} = \mathbf{L}\mathbf{x} \tag{1}$$

where $\mathbf{x}$ is a column vector, the superscript $\dot{}$ represents the time derivative, and $\mathbf{L}$ is a matrix with periodic coefficients which have time period T. If $\mathbf{x}_0(t)$ is a solution of equation (1), it is easy to see that if

$$\mathbf{x}_0(t + (n+1)T) = \mathbf{A}\mathbf{x}_0(t + nT) \tag{2}$$

where n is an integer, then

$$\mathbf{A} = \exp\left(\int_t^{t+T} dt' \mathbf{L}(t')\right) = \exp(\mathbf{B}) \tag{3}$$

where B is a square matrix. In addition, it can be easily inferred that if all eigenvalues of $\mathbf{A}$ are discrete and $\mathbf{A}$ is non-singular so that it can be reduced to its Jordan form, the eigenvectors of $\mathbf{B}$ are identical to the eigenvectors of $\mathbf{A}$, and α_i, the eigenvalues of $\mathbf{A}$, are related to θ_i, the eigenvalues of $\mathbf{B}$, by

$$\alpha_i = \exp(\theta_i). \tag{4}$$

The eigen values of $\mathbf{A}$ determine whether the components of the vector $\mathbf{x}_0$ decay or grow as time progresses. If any eigenvalue of $\mathbf{A}$ is greater than 1 (or any eigenvalue of $\mathbf{B}$ is positive), then the projection of $\mathbf{x}_0$ in the direction of the corresponding eigenvector of $\mathbf{A}$ increases as the number of time periods increases, whereas if all eigenvalues $\mathbf{A}$ are less than 1 (or all eigenvalues of $\mathbf{B}$ have negative real parts), then all components of $\mathbf{x}_0$ decay in time. For a steady flow in which $\mathbf{L}$ is independent of time, the eigenvalues θ_i of $\mathbf{B}$ are related to the eigenvalues λ_i of L (the linear growth rates) by

$$\theta_i = \frac{\lambda_i}{T}. \tag{5}$$

The stability of an oscillatory flow which satisfies the equation

$$\dot{\mathbf{x}}(t) = F(\mathbf{x}(t)) \tag{6}$$

is determined as follows. First, the time periodic solution $\bar{\mathbf{x}}$ which satisfies the equation (6) is identified. The solution is then perturbed about this state using a perturbation of the form $\mathbf{x} = \bar{\mathbf{x}} + \mathbf{x}'$, and the equation (6) is linearized in the amplitude of the perturbations $\mathbf{x}'$ to obtain an equation of the form

$$\dot{\mathbf{x}}' = \mathbf{L}\mathbf{x}'. \tag{7}$$

Equation (7) is then reduced to an equation of the form 2, and the eigenvalues of the matrix $\mathbf{A}$ (or equivalently the Floquet exponents, which are the eigenvalues θ_i of the matrix $\mathbf{B}$) are extracted to determine the stability of the time periodic state. In the present work, we discuss the stability characteristics in terms of the eigenvalue θ_i, the growth rate of the system. The system is stable if the growth rate θ_i is negative and unstable if θ_i is positive.

3 Spring backed plates

The flow of a fluid between a spring backed flexible wall at $z^* = 0$ and a rigid plate at $z^* = H^*$ is considered, and the spring backed wall is at rest in the base state, while the rigid wall moves with a velocity $V^* + A^* \cos(\Omega^* t^*)$, where V^* is the steady velocity, Ω^* is the dimensional frequency of the top plate, and A^* is the dimensional amplitude of the top plate. The superscript * is used to indicate dimensional quantities, while quantities without the superscript are dimensionless. The fluid is an incompressible Newtonian fluid with density ρ^* and viscosity μ^*, and the wall is

modeled as a spring backed wall in which the springs are inclined, so that the wall has both normal and tangential compliance. No-slip conditions are used for the fluid velocity at both surfaces, while the stress balance condition at the flexible wall is

$$\mathbf{n}^*.\mathbf{T}^*.\mathbf{n}^* = \left[M^*\partial_t^{*2} - T^*\partial_x^{*2} + B^*\partial_x^{*4} + K^*\right] u_z^* \quad (8)$$

$$\mathbf{t}^*.\mathbf{T}^*.\mathbf{n}^* = \left[M^*\partial_t^{*2} - E^*\partial_x^{*2} + K^*\right] u_x^* \quad (9)$$

where $\mathbf{T}^*$ is the stress tensor in the fluid, $\mathbf{n}^*$ and $\mathbf{t}^*$ are the unit normal and tangent to the surface, M^*, T^*, B^*, K^* and E^* are the dimensional mass, transverse tension, bending modulus, spring constant and longitudinal tension respectively, u_z^* and u_x^* are the normal and tangential displacements respectively, and x^* and z^* are the coordinates tangential and normal to the surface in the base state.

The spring backed wall model is similar to that used by Thaokar et al. [24] and Shankar and Kumaran [25], which is a slight modification of the model used in earlier studies [8–12]. In these models, the normal force in the wall is proportional to normal displacement, but there is no equivalent restoring force in the tangential direction. In the absence of a tangential restoring force proportional to tangential displacement, the surface develops a longitudinal tension due to the steady mean flow which increases in the flow direction. In the present analysis, a tangential restoring force proportional to the tangential displacement is included, to balance the mean stress exerted due to the fluid shear at the surface.

The fluid velocity field is scaled by $(H^{*2}K^*/\mu^*)$, length is scaled by H^*, time by (μ^*/H^*K^*) and pressure by (K^*H^*). The scaled top plate mean velocity is then given by $\Lambda + A\cos(\Omega t)$, where the non-dimensional strain rates are $\Lambda = (V^*\mu^*/H^{*2}K^*)$ and $A = (A^*\mu^*/H^{*2}K^*)$. The non-dimensional membrane parameters are $M = M^*/(\rho^*H^*)$, $E = E^*/(K^*H^{*2})$, $T = T^*/(K^*H^{*2})$ and $B = B^*/(K^*H^{*4})$. The non-dimensional Navier-Stokes equations are

$$\nabla.\mathbf{v} = 0 \quad (10)$$

$$\Sigma\left(\partial_t\mathbf{v} + \mathbf{v}.\nabla\mathbf{v}\right) = -\nabla P + \nabla^2\mathbf{v} \quad (11)$$

where $\mathbf{v}$ is the fluid velocity field, P is the pressure field, $\Sigma = \frac{Re}{\Lambda} = \frac{Re_o}{A}$, and the two Reynolds numbers Re and Re_o based on the steady mean velocity and the oscillatory mean velocity are $Re = \frac{\rho^*V^*H^*}{\mu^*}$ and $Re_o = \frac{\rho^*A^*H^*}{\mu^*}$ respectively. Note that Σ is a material property which is independent of velocity, given by $\Sigma = \frac{\rho^*H^{*3}K^*}{\mu^{*2}}$. The base state velocity profile is a unidirectional, time periodic flow in the fluid, and the base state tangential displacement is time periodic, both of which have frequency Ω. The velocity profile in the base state in the flow direction, $\bar{v}_x$, is governed by the momentum equation

$$\Sigma\frac{\partial\bar{v}_x}{\partial t} = \frac{\partial^2\bar{v}_x}{\partial z^2} \quad (12)$$

and the boundary conditions are

$$\bar{v}_x|_{z=1} = \Lambda + A\cos(\Omega t)$$

$$\bar{v}_x|_{z=0} = \frac{d\bar{u}_x}{dt}$$

$$\frac{d\bar{v}_x}{dz}|_{z=0} = \frac{ReM}{\Lambda}\frac{d^2\bar{u}_x}{dt^2} + \bar{u}_x \quad (13)$$

where $\bar{u}_x$ is the mean tangential displacement in the wall.

In the normal mode analysis, the perturbation variables are expressed as $f(x,z,t) = \tilde{f}(z,t)e^{ikx}$, where k is the wave number in the streamwise direction. An Orr-Sommerfeld type of equation can then be obtained for the perturbation to the fluid velocity field,

$$\Sigma\left[\frac{\partial}{\partial t} + \bar{v}_x ik\right](\partial_z^2 - k^2)\tilde{v}_z = (\partial_z^2 - k^2)^2\tilde{v}_z + \Sigma\, ik(\partial_z^2\bar{v}_x)\,\tilde{v}_z. \quad (14)$$

The boundary conditions for this equation at the top plate are $\tilde{v}_z = 0$ and $\partial_z\tilde{v}_z = 0$ ($\tilde{v}_x = 0$). The boundary conditions at the spring backed plate membrane are

$$\tilde{v}_z = \partial_t\tilde{u}_z + \bar{v}_x ik\tilde{u}_z, \quad (15)$$

$$\tilde{v}_x + \tilde{u}_z\partial_z\bar{v}_x = \partial_t\tilde{u}_x + \bar{v}_x ik\tilde{u}_x \quad (16)$$

$$\partial_z\tilde{v}_x + ik\tilde{v}_z + \partial_z(\partial_z\bar{v}_x)\tilde{u}_z = \left[\Sigma M\partial_t^2 + Ek^2 + 1\right]\tilde{u}_x \quad (17)$$

$$-\tilde{p} + 2\partial_z\tilde{v}_z - (\partial_z\bar{v}_x)ik\tilde{u}_z = \left[\Sigma M\partial_t^2 + Tk^2 + Bk^4 + 1\right]\tilde{u}_z \quad (18)$$

where

$$\tilde{p} = \frac{i}{k}\Sigma\left[\left(\frac{\partial}{\partial t} + \bar{v}_x ik\right)\tilde{v}_x + (\partial_z\bar{V}_x)\,\tilde{v}_z\right] - \frac{i}{k}(\partial_z^2 - k^2)\tilde{v}_x. \quad (19)$$

It should be noted that the results of the linear stability analysis for a steady shear flow for the present spring model equation (9) are qualitatively different from earlier results [24,25] due to the presence of the tangential restoring force. Whereas the scaled transition velocity Λ is proportional to k in the low wave number limit in the earlier studies [24,25], the transition velocity converges to a finite value in the limit $k \to 0$ in the present case, due to the tangential restoring force, as shown in Figure 1.

The stability of the oscillatory flow was studied using asymptotic analysis, as well as numerically using the Chebushev Tau method [23,27]. The spectral Chebyshev Tau method is verified with the analytical results at zero Reynolds number and with the numerical results obtained by the method of Srivatsan and Kumaran [26], and good agreement was found upto five significant figures. The spectral code for the oscillatory problem was also validated by comparing with the zero Reynolds number asymptotic analysis for the oscillatory case, and good agreement was found.

The steady flow over spring backed wall shows a zero Reynolds number, low wavenumber instability when the top plate velocity exceeds a critical velocity, and this critical velocity approaches a constant value in the zero wavenumber limit. It is of interest to see if such an instability also exists for the case of purely oscillatory flows.

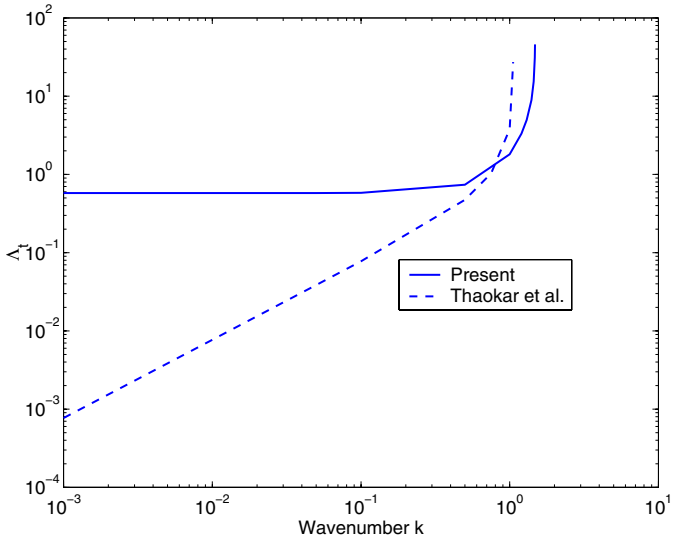

Fig. 1. Effect of tangential spring restoring force on the neutral stability curve in the absence of oscillation ($Re = 0$, $M = T = B = K = E = 1$).

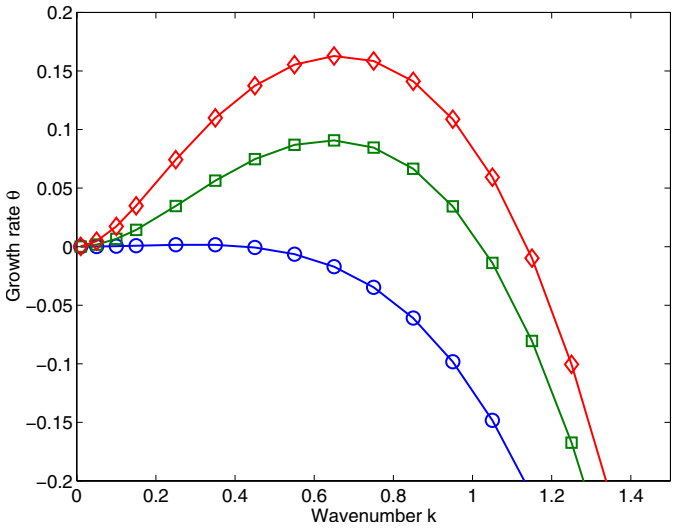

Fig. 2. Growth rate θ vs. k for the case of purely oscillatory flow over spring backed walls ($\diamond\Omega = 0.5$, $\square\Omega = 1.0$, $\bigcirc\Omega = 2.0$, A=5.0, $Re = 0$, $M = T = B = K = E = 1$, $\Lambda = 0$).

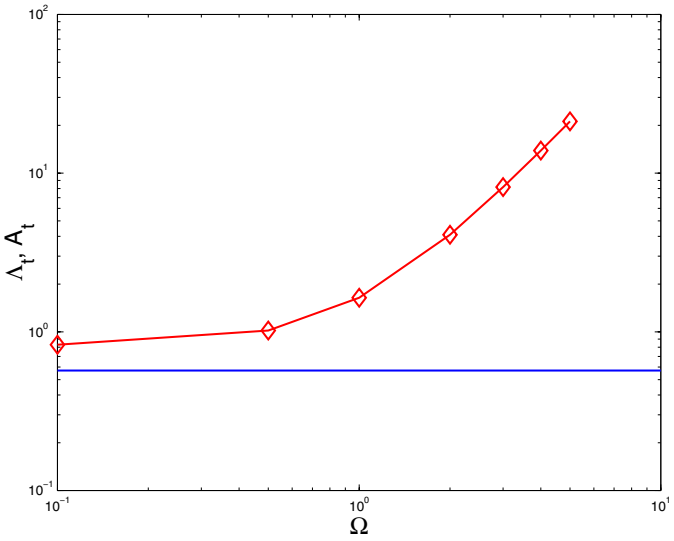

Fig. 3. Effect of frequency on the asymptotic destabilizing oscillatory amplitude in the low wavenumber A vs. Ω for an oscillatory base velocity. The solid line indicates Λ_t for the steady base velocity, the line with symbol $\diamond$ is for an oscillatory base velocity, $Re = 0$, $M = T = B = K = E = 1$, $\Lambda = 0$, $k = 0.001$).

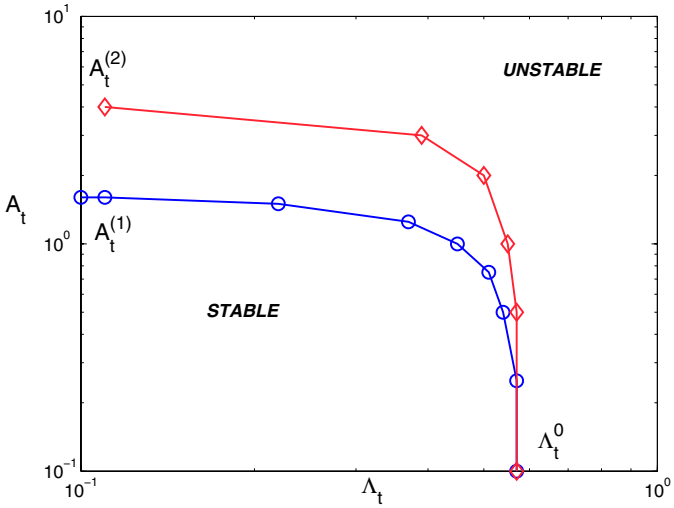

Fig. 4. Stability regime in the Λ_t-A_t plane for $\bigcirc\Omega = 1$, $\diamond\Omega = 2.0$ ($Re = 0$, $M = T = B = K = E = 1$, $k = 0.001$).

Figure 2 shows the variation of the real part of growth rate with the wavenumber in the absence of steady shear. The figure shows that for the case of purely oscillatory flows, the system shows that the growth rate scales as k^2 in the $k \to 0$ limit. The growth rate and the wavenumber corresponding to the most unstable mode both decrease with increasing frequency. This shows that an increase in the frequency of oscillations stabilises the flow. The effect of frequency on the transition velocity of an oscillatory flow in the low wavenumber limit is shown in Figure 3. The transition velocity increases with an increase in the oscillating frequency, indicating that the system is stabilised at higher frequencies.

The stable and unstable domains in the $A_t - \Lambda_t$ plane are shown as a function of frequency in Figure 4. The figure shows that the neutral stability curves for the steady and oscillatory instabilities are connected, so that there is a transition from the steady to the oscillatory instability as Λ is decreased from the transition value to zero and A is increased from zero the transition value.

It is of interest to examine the continuation of the instability of an oscillatory flow in the finite Reynolds number regime. In the case of a steady flow past a spring backed plate model [29], the transition Reynolds number increases proportional to Σ at low Reynolds number, but increases proportional to $\Sigma^{1/2}$ in the high Reynolds number limit, as shown in Figure 5. Figure 5 also shows the neutral stability curves for a purely oscillatory flow which are continuations of the neutral stability curves in the zero

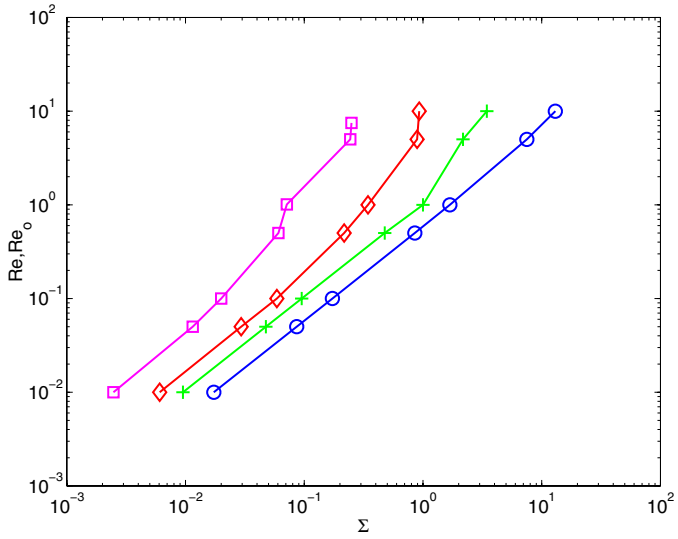

Fig. 5. Variation of Re vs. Σ and Re_o vs. Σ for steady and oscillatory flows over a spring backed plate ($\square\Omega = 2.0$, $\diamond\Omega = 1.0$, $+\Omega = 0.5\bigcirc$ Steady base velocity, $M = T = B = K = E = 1$, $k = 0.01$).

Reynolds number limit. It is observed that the transition Reynolds number for the oscillatory flow is proportional to Σ at low Reynolds number for all the frequencies studied, and this scaling relation is identical to that for a steady flow. However, the transition Reynolds number Re_{ot} diverges at higher values of Σ, in contrast to the $\Sigma^{1/2}$ scaling for the steady flow. This implies that the oscillatory flow becomes unstable only when Σ is below a critical value at a given frequency, and there is no instability when Σ increases beyond this value. Figure 5 also shows that the transition Reynolds number increases as the frequency is increased at a fixed value of Σ, indicating that the flow is stabilised as the frequency is increased.

4 Oscillatory flow over viscoelastic gels

The configuration consists of an incompressible viscoelastic gel of thickness HR^* grafted to a rigid surface, and an incompressible Newtonian fluid layer of thickness R^* between the gel surface and a rigid top plate. In this case, the material parameters that affect the dynamics of the system are the density of the fluid and gel ρ^* (assumed to be equal), the shear modulus E^* and viscosity μ_g^* of the gel, in addition to the fluid viscosity μ^*. The velocity is scaled by (E^*R^*/μ^*), the length by (R^*), time by (μ^*/E^*), the pressure by (E^*), and the relative viscosity $\eta_g = (\mu_g^*/\mu^*)$ is defined as the ratio of the viscosity of the gel and fluid. The nondimensional top velocity is then given by $\Lambda + A\cos(\Omega t)$, where the non dimensional strain rates are $\Lambda = (V^*\mu^*/E^*R^*)$ and $A = (A^*\mu^*/E^*R^*)$.

The scaled equations for the fluid are the incompressible Navier-Stokes equations

$$\nabla.\mathbf{v} = 0 \tag{20}$$

$$\Sigma_g\left(\partial_t\mathbf{v} + \mathbf{v}.\nabla\mathbf{v}\right) = -\nabla P^f + \nabla^2\mathbf{v} \tag{21}$$

where $\Sigma_g = \frac{Re}{\Lambda} = \frac{Re_o}{\Lambda} = \frac{\rho^* R^{*2} E^*}{\mu^*}$, $Re = \frac{\rho^* V^* H^*}{\mu^*}$, and $Re_o = \frac{\rho^* A^* H^*}{\mu^*}$ are the steady and oscillatory Reynolds numbers. The equations for the displacement field in the gel, $\mathbf{u}$, which represents the displacement of material points from their steady state positions due to the stresses exerted on the gel, are [17–20]

$$\nabla.\mathbf{u} = 0 \tag{22}$$

$$\Sigma_g\,\partial_t^2\mathbf{u} = -\nabla P^g + (1+\eta_g\partial_t)\nabla^2\mathbf{u}. \tag{23}$$

The base state velocity profile is governed by the equation

$$\Sigma_g\frac{\partial\bar{v}_x}{\partial t} = \frac{\partial^2\bar{v}_x}{\partial z^2} \tag{24}$$

and the governing equation for the mean gel displacement is given by

$$\Sigma_g\frac{\partial^2\bar{u}_x}{\partial t^2} = \left(1+\eta_g\frac{\partial}{\partial t}\right)\frac{\partial^2\bar{u}_x}{\partial z^2} \tag{25}$$

where $\mathbf{u}$ is the displacement field, which represents the displacement of material points from their steady state positions due to stresses exerted on the gel. The boundary conditions are

$$\begin{aligned}
\bar{v}_x|_{z=1} &= \Lambda + A\cos(\Omega t)\\
\bar{v}_x|_{z=0} &= \frac{d\bar{u}_x}{dt}|_{z=0}\\
\frac{d\bar{v}_x}{dz}|_{z=0} &= \left(1+\eta_g\frac{\partial}{\partial t}\right)\frac{d\bar{u}_x}{dz}|_{z=0}\\
\bar{u}_x|_{z=-H} &= 0
\end{aligned} \tag{26}$$

where $\bar{u}_x$ is the mean displacement in the wall. It should be noted that the base state is characterised by an oscillatory fluid velocity as well as an oscillatory gel displacement field.

The calculation of the growth rate is similar to that for the spring backed wall model, and is not discussed in detail. First, the limit $Re = 0$ and $Re_o = 0$ is considered, where the scaled wave number and frequency are $O(1)$, and $St = \Sigma_g\Omega = 0$. For a purely oscillatory flow, the low Reynolds number asymptotic analysis for this system indicates that the system indeed becomes unstable when the top plate velocity amplitude exceeds a critical value. Figure 6, which shows the transition amplitude as a function of the wavenumber k, indicates that the critical wavenumber is not significantly altered by the oscillations. However the value of critical amplitude initially increases with the increasing frequency, and then decreases at very high frequencies. This figure shows that the critical value of the oscillation amplitude is higher than the critical strain rate required for the non-oscillatory case. The neutral stability curves at the critical wavenumber k_c for the purely oscillatory flows for three different gel thicknesses are shown in the Figure 7. For a steady flow, the transition velocity is a decreasing function of the gel thickness. However, for an oscillatory flow, it is observed that the transition velocity is a decreasing function of the gel thickness at low

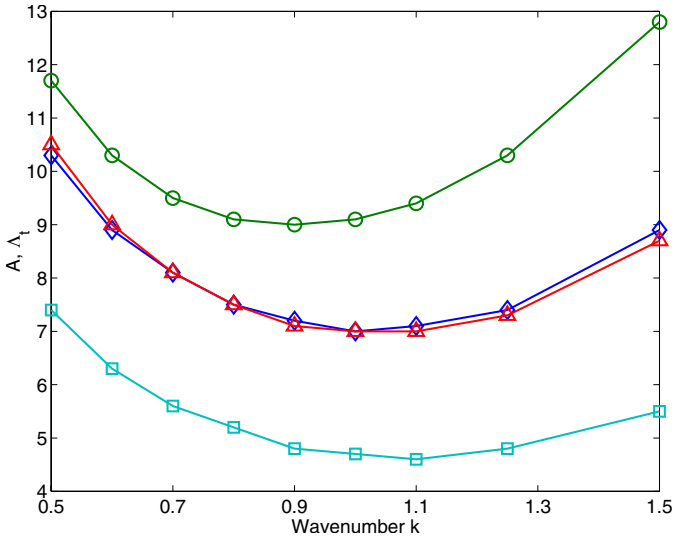

Fig. 6. Critical amplitude for low Reynolds number unstable modes for flow over a gel. $\diamond\Omega = 1.0$, $\bigcirc\Omega = 5.0$, $\triangle\Omega = 0.5$, $\square$ Steady mean flow, $\Sigma_g = 0.00025, H = 1, \gamma = 0.0$, $\eta_g = 0$.

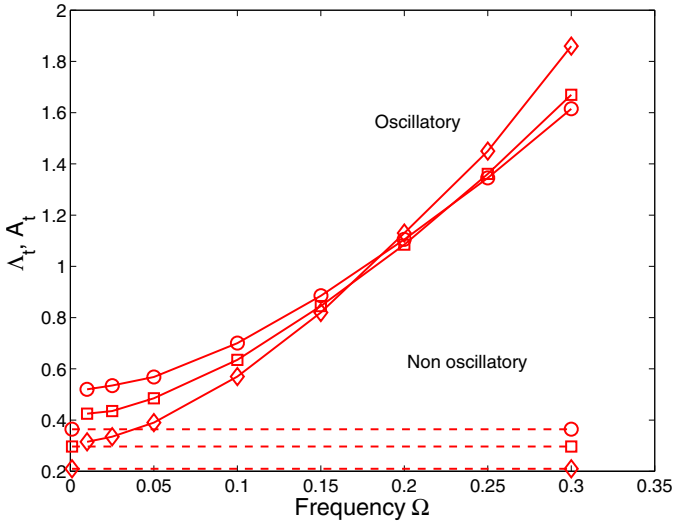

Fig. 7. Neutral curves for the steady and oscillatory base flows for $\gamma = 0$, $\diamond$ H = 15 ($k_c = 0.1$), $\square$ H = 11 ($k_c = 0.15$), $\bigcirc$ H = 9 ($k_c = 0.2$), $\eta_g = 0$.

frequencies, but becomes an increasing function as the gel thickness is increased. The low Reynolds number results are compared with experimental observations in the following Section 5.

We now consider the stability of an oscillatory velocity superimposed on a steady velocity of the top plate at two different values of the non-dimensional parameter Σ_g, which is a function only of the physical properties of the system, which show that oscillations have a qualitatively different effect on the stability in the low and intermediate Reynolds number regimes. The system is known to exhibit a low Reynolds number instability for a steady base flow, and the critical wave number is comparable to the inverse of the fluid thickness for a fixed value of the parameter

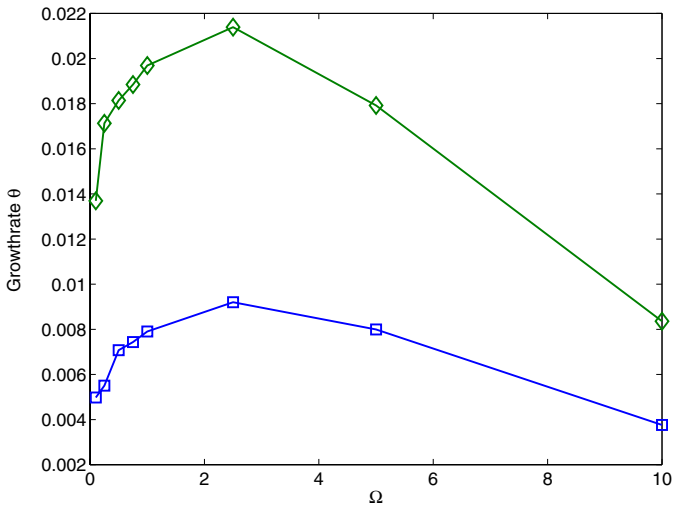

Fig. 8. Effect of oscillation frequency on the growth rate of the instability of the steady flow past a gel at low Reynolds number ($\square A = 0.5\Lambda$, $A = 0.75\Lambda, \Sigma_g = 0.025$ $H = 1$ $Re = 0.11$, $k = 1.1, \eta_g = 0$).

Σ_g. The transition Reynolds number scales as $Re \sim \Sigma_g$ in the low Reynolds number regime. We consider three values of the parameter $\Sigma_g = 0.025$, 1.0 and 10.0, corresponding to transition Reynolds number 0.11, 4.738 and 37.2 respectively, in the low and intermediate Reynolds number ranges.

The effect of plate oscillation on the growth rate is examined in Figure 8 for $\Sigma = 0.25$ when the strain rate in the steady flow is 0.11 and the wave number is $k_c = 1.1$. This figure shows that plate oscillations increase the growth rate, and have a destabilizing effect. The growth rate is also found to increase with an increase in the amplitude of oscillations. The dependence on the frequency is more complex, since the growth rate first increases and then decreases with frequency. The above results indicate that in the low Reynolds number regime, the critical strain rate is reduced in the presence of plate oscillation.

The effect of plate oscillations on the growth rate $\Sigma = 1.0$, $Re_t = 4.738$ and critical wave number $k_c = 1.1$ are shown in Figure 9. This figure shows that the plate oscillations have a complicated effect on the growth rate in this parameter regime. Wall oscillations are found to have a stabilising effect at high frequencies and destabilizing at lower frequencies. The system shows a maximum in the growth rate at an intermediate frequency. The growth rate is also found to increase with an increase in the amplitude of oscillations.

The dependence of the transition velocity on the frequency of oscillations is more complicated at high Reynolds number, due to the non-monotonic dependence of the mean strain rate at the interface on the frequency of oscillations. Figure 10 shows the variation of growth rate of a neutrally stable non-oscillatory mode with frequency for two different wall amplitudes. The plot shows a strong destabilizing effect at a oscillation frequency of $\Omega = 1.5$. The reason for this is the non-monotonic variation of the amplitude of the velocity oscillations in the mean flow at

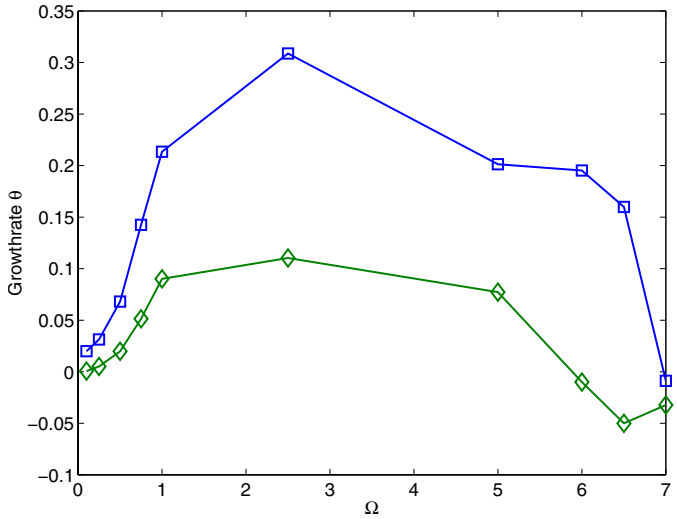

Fig. 9. Effect of oscillation frequency on the growth rate of the steady flow past a gel, $\square A = 0.7\Lambda$, $A = 0.5\Lambda$, $\Sigma_g = 1.0$, $H = 1$, $Re = 4.676$, $k = 1.1, \eta_g = 0$.

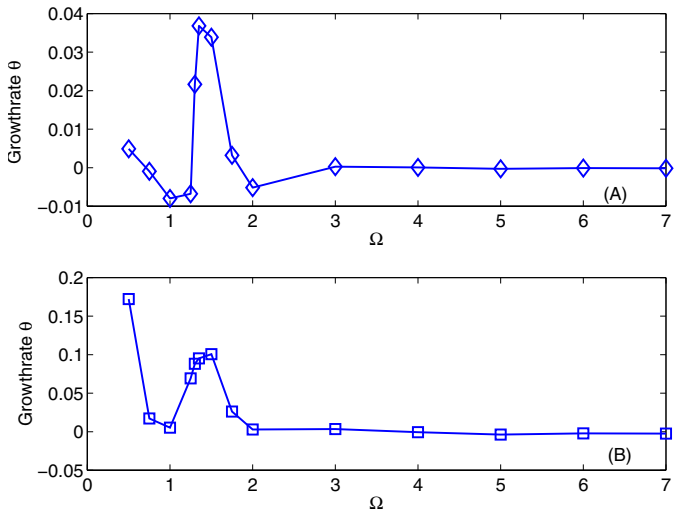

Fig. 10. Variation of growth rate with oscillation frequency for two different amplitudes of the oscillatory velocity, (a) $A = 0.25\Lambda$, (b) $A = 0.5\Lambda$, for $\Sigma_g = 10.0$, $H = 1$, $Re = 37.27$, $k = 1.75$, $\eta_g = 0$.

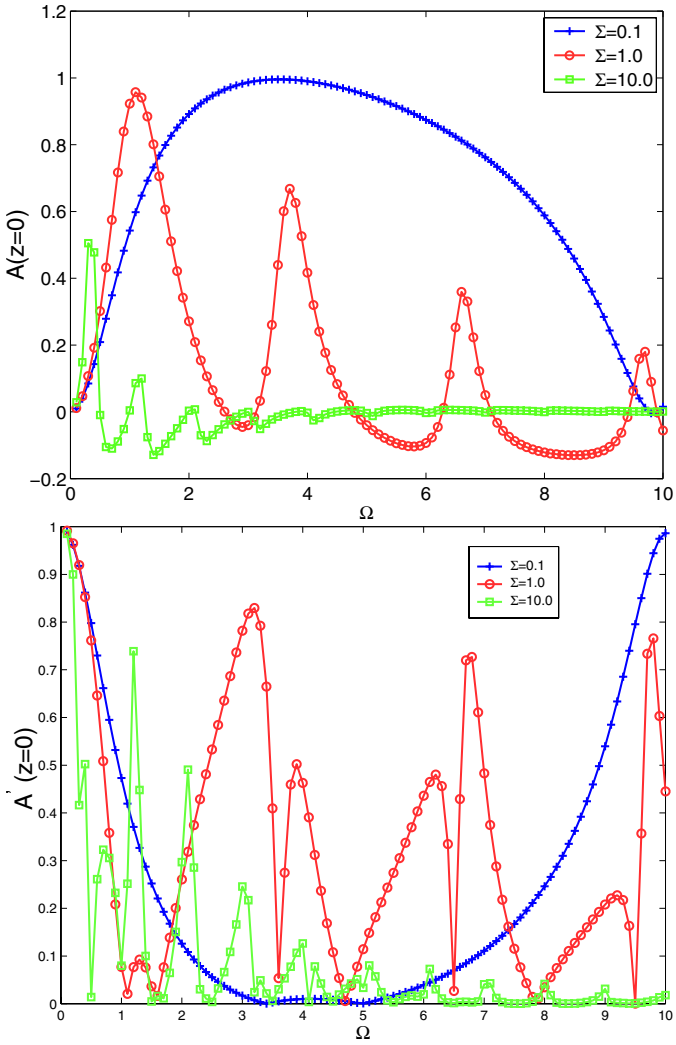

Fig. 11. The amplitude of the velocity fluctuations A, and the derivative of A with respect to the z cordinate A', as a function of the oscillation frequency Ω for different values of Σ_b. ($+\Sigma_g = 0.1$, $\square\Sigma_g = 1.0$, $\square\Sigma_g = 10.0$, $H = 1$, $\gamma = 2.0, \eta_g = 0$).

the interface between the fluid and the gel, due to the complex coupling between the fluid and gel dynamics. If the amplitude of the velocity oscillations at the interface A is plotted as a function of frequency Ω, as shown in Figure 11, the amplitude increases and then decreases for $\Sigma = 0.1$, but shows a complicated non-monotonic variation at $\Sigma = 1.0$ and 10.0. The amplitude of the strain rate at the interface $A'(z = 0)$, which is the normal derivative of the velocity, also shows complicated behaviour. Our calculations show that the positions of the peaks in the $s - \Omega$ curve coincide with the positions of the peaks in the $A' - \Omega$ curves, indicating that the high growth rates are due to the large strain amplitudes at this interface. It is important to note that this type of behaviour is not observed in the spring backed wall model, since the velocity amplitude is a monotonic function of the frequency in that case, and so the complicated behaviour of the growth rate with frequency is not observed in that case.

5 Experimental studies

The experiments were carried out using an AR-1000N rheometer with a parallel plate geometry. Polyacrylamide gel was used as the flexible surface, and silicone oil was used as the fluid. The method of preparation and characterisation of the gel was identical to that in earlier experiments of Muralikrishnan and Kumaran [21,22], and so these are not repeated here. In the experiments, the polyacrylamide gel of thickness about 4 mm was placed on the bottom plate of the rheometer. Silicone oil was placed on the gel, and the top plate was lowered to obtain a film of thickness about 300 μm. In earlier studies [21,22], the instability of a steady flow was inferred as follows. The top

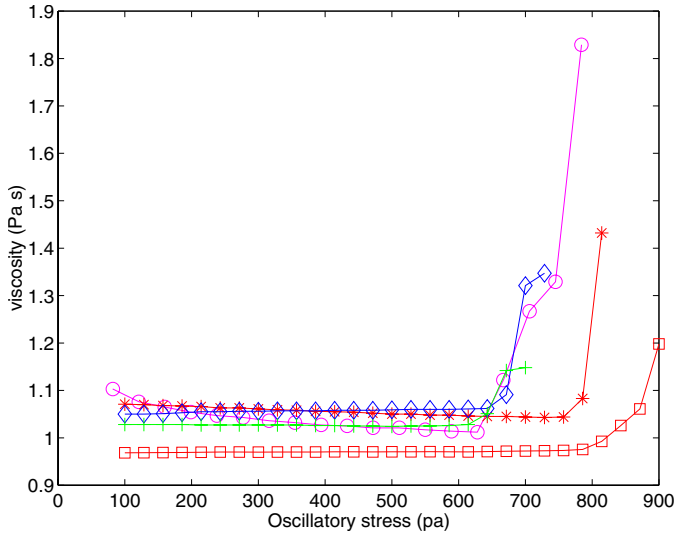

Fig. 12. Viscosity as a function of stress amplitude for $H = 4709$ μm, $G = 2205$ Pa, $\eta = 1.0$ Pa s, $R = 300$ μm, ◯ Steady flow, $*\Omega = 0.0028, \diamond\Omega = 0.0057, +\Omega = 0.0142, \square\Omega = 0.0214$.

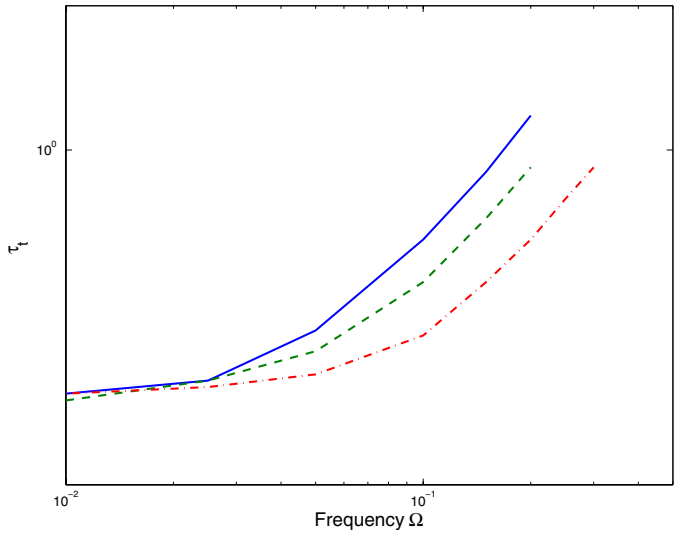

Fig. 13. Critical stress amplitude vs. frequency for $H = 15$ for different gel viscosities, (—($\eta_g = 16.0$), - - - -($\eta_g = 10$), —·—·($\eta_g = 5.0$)).

plate was rotated in the stress-controlled mode, and the shear stress was progressively increased. In the rheometer, the torque and angular velocity of the top plate are measured, and the shear stress and strain rate at the outer edge of the top plate are calculated *assuming the flow is laminar*. If a Newtonian fluid is placed between the two surfaces, the viscosity is independent of the shear stress. However, when the bottom plate is flexible, there is a viscous instability when the strain rate exceeds a critical value, and the flow undergoes a transition from a laminar flow to a more complicated velocity profile. Since this more complicated velocity profile has a higher dissipation, the apparent viscosity (ratio of the shear stress to strain rate assuming the flow is laminar) is higher than the intrinsic viscosity of the fluid. Since the shear stress is fixed and the apparent viscosity increases, the strain rate decreases after transition. The point at which the viscosity increases provides the strain rate for the onset of instability. In the present experiments, an oscillatory stress was superimposed on the steady stress, and the viscosity was measured as a function of strain rate. The presence of an instability was inferred as discussed above, and a typical viscosity-shear stress curve showing the onset of instability is shown in Figure 12.

The oscillatory experiment was repeated at different frequencies for the same sample, and care was taken to ensure that the experiment was stopped before there is significant damage to the surface of the gel due to the instability. After the oscillation experiments are over, the stability of a steady flow was measured using a steady stress ramp, where the stress is increased at a constant rate and the viscosity. The observation of the instability of the steady flow at the stress predicted by theory was used to indicate that the surface of the gel is not damaged by the flow.

Since the experiments are conducted under constant stress conditions, it is necessary to modify the Floquet analysis to calculate the critical stress required for the onset of instability, rather than the critical strain rate which was calculated in the previous section. This calculation is easily carried out, and is not explained in detail here. It is important to note, however, that the results show a strong dependence of the transition stress on the gel viscosity. For example, the effect of gel viscosity on the transition stress, shown in Figure 13, indicates that there is a significant difference in the critical stress for the oscillatory instability when the viscosity ratio is increased from 5 to 16, though there is less variation in the critical stress for a steady flow in the zero frequency limit. The gel viscosity could not be determined from experiments, since the loss modulus of the soft gels used in the experiments could not be determined due to limitations in the oscillatory measurements. In order to compare the theory with experiments, the viscosity ratio has been set equal to 16, since this value is consistent with the theoretical predictions for the critical stress for a steady flow. However, the sensitive dependence of the critical stress on the viscosity ratio should be kept in mind while interpreting the results.

Figures 14 and 15 show the experimental results for two different nondimensional H values, $H = 15$ and $H = 9$, which in the present case correspond to fluid thicknesses of 300 μm and 500 μm respectively. The different data sets in the plots correspond to different gel thicknesses and shear moduli. The results are compared with the theoretical results obtained using the procedures in Section 5. These figures show the theoretical predictions for the critical stress for a steady flow, as well as the frequency dependence of the critical stress for an oscillatory flow. The experimental results show significant scatter, but are consistent with a transition from the critical stress for a steady flow to that for an oscillatory flow as the frequency increases. This is expected for the following reason. At low frequencies, the growth rates corresponding

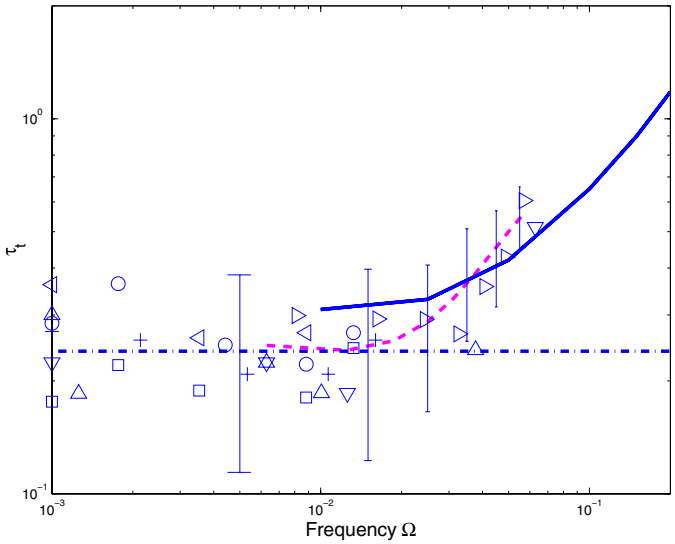

Fig. 14. Critical stress amplitude vs. frequency for $H = 15$, —theoretical prediction steady base flow with $\eta_g = 16$, – · – · theoretical prediction steady base flow with $\eta_g = 16$, - - - - best fit of experimental data, $\square H = 4614, G' = 3500, \bigcirc H = 4600, G' = 3560, + H = 4600, G' = 2945, \triangle H = 4400, G' = 500, \triangledown H = 4600, G' = 600, \triangleright H = 4721, G' = 700, \triangleleft H = 4702, G' = 1000, \diamond H = 4525, G' = 1250$).

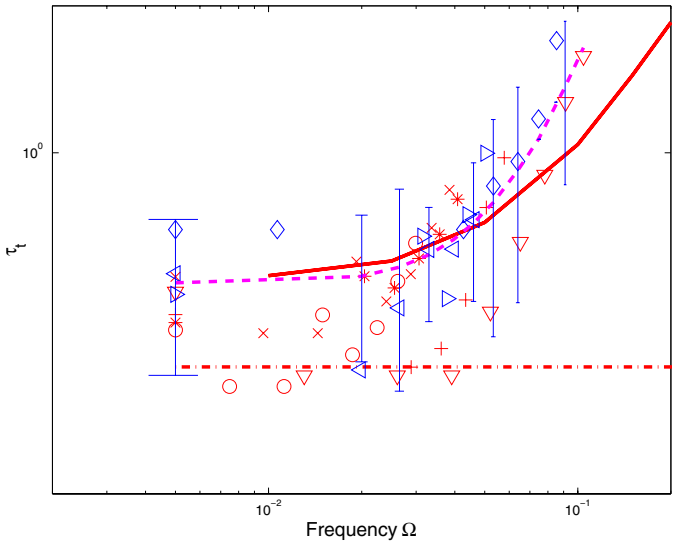

Fig. 15. Critical stress amplitude vs. frequency for $H = 9$, —theoretical prediction oscillatory base flow with $\eta_g = 16$, – · – · theoretical prediction steady base flow with $\eta_g = 16$, - - - - best fit for experimental results, $* H = 4728, G' = 1230, \triangledown H = 4720, G' = 482, + H = 4637, G' = 869, X H = 4627, G' = 1307, \bigcirc H = 4746, G' = 1681, \diamond H = 4701, G' = 589, \triangle H = 4714, G' = 3500, \triangleright H = 4715, G' = 1000, \triangleleft H = 4043, G' = 950$).

to the steady flow instability is much larger than the time scales of the oscillation, and the mean flow at any instant of time can be considered to be a steady Couette flow driven by the stress exerted by the top plate. In this case, it is expected that the onset of instability occurs when the maximum stress at the top plate exceeds the critical stress for a steady flow required for the onset of instability. As the frequency is increased, the growth rate of perturbations is not large compared to the frequency of oscillations, and the growth of fluctuations when the top plate stress is greater than the steady critical stress is offset by the decay of fluctuations when the top plate stress is lower than the steady critical stress. In this case, it is expected that the instability is due to the accumulated growth of perturbations over many cycles, which is studied in the Floquet analysis conducted here.

There is significant scatter in the data for many reasons. The gels used here are soft, with shear modulus between 400 and 3000 Pa. In this case, it is difficult to get an accurate estimate of the gel thickness, because the gel gets significantly compressed when the zero gap adjustment is made. Since the gel is about 10 times thicker than the fluid film, an error of 1% in the gel thickness could result in a variation of 10% in the fluid thickness, thereby resulting in an error in the theoretical estimate of the critical strain rate. In addition, as noted before, there is a sensitive dependence of the critical stress on the viscosity ratio. Despite these uncertainties, it is clearly seen that there is a transition from the critical stress for a steady flow to the critical stress for the oscillatory flow as the frequency is increased, and the predicted increase in the critical stress with frequency is clearly observed in the experiment. When the critical stress is averaged over all the experimental runs, there is agreement between the theoretical and experimental results with no fitting parameters, apart from the gel viscosity which was fitted to obtain agreement for the steady flow.

6 Conclusions

The effect of plate oscillations on fluid flow over compliant surfaces was studied numerically and analytically using the Floquet analysis. Two types of compliant surfaces were studied, the spring backed wall model, which allows for tangential motion of the surface, and the incompressible viscoelastic gel model. Both the spring backed wall model and the viscoelastic gel model show a purely oscillatory instability in the limit of zero Reynolds number, and the system is stabilised by an increase in frequency. The transition velocity amplitude for oscillatory instability has a minimum at zero Reynolds number for the spring backed model, whereas it has a minimum at finite wavenumber for the viscoelastic gel model. For the spring backed plate model, the continuation of the neutral stability curve at small but finite Reynolds number is studied, and it is found that the transition oscillatory Reynolds number increases as $Re_o \sim \Sigma$, in a manner similar to the increase of the transition Reynolds number for a steady mean flow. However, it is found that the qualitative behavior in the high Reynolds number limit is very different. Whereas the critical Reynolds number for a steady flow increases proportional to $\Sigma^{1/2}$ in the high Reynolds number limit, it is found that the critical Reynolds number for an oscillatory flow diverges at a finite value of Σ. It

is shown that the instability due to steady mean flow and the purely oscillatory instability reinforce each other, and the region of instability for a combination of oscillatory and steady flow identified on a $\Lambda - A$ parameter space.

The effect of plate oscillations was studied on the low Reynolds number instability in steady flow over finite thickness viscoelastic gels. The steady flow past a viscoelastic gel is known to exhibit a low Reynolds number instability, and the transition velocity has a minimum at finite wave number. A similar instability is encountered for the oscillatory flow past a viscoelastic gel, but the dependence of the transition velocity amplitude on the frequency was found to be complicated. At low Reynolds number, the velocity amplitude for an oscillatory flow was found to be lower than that for a steady flow at all wave numbers, and the transition amplitude was found to increase with frequency. However, at higher Reynolds numbers, the transition amplitude for an oscillatory flow was found to be lower than that for a steady flow for certain wave numbers, indicating a destabilizing effect. It was also found that wall oscillations could have a complicated effect on the instability at intermediate and high Reynolds numbers, because of the complicated and non-monotonic dependence of the interfacial mean velocity amplitude on the frequency. It should be noted that the qualitative nature of the neutral curves for a viscoelastic gel model cannot be adequately reproduced using the spring-backed wall model due to the non-monotonic nature of the growth rate-frequency curves in the gel model. This is in contrast to the case of steady flow past a flexible surface, where the qualitative behaviour of the neutral curves for the viscoelastic model can be adequately reproduced in a spring-backed wall model by tuning the parameters. This indicates that accurate representation of the wall dynamics is more critical for oscillatory flows. Experiments were carried out on the stability of an oscillatory flow past a viscoelastic gel in the zero Reynolds number limit, and the results were in qualitative agreement with the theoretical predictions, though it should be noted that there is considerable scatter in the experimental results, for reasons explained in Section 5.

References

1. David. N. Ku., Ann. Rev. Fluid Mech. **29**, 399 (1997)
2. C.-S. Yih, J. Fluid Mech. **31** 737 (1968)
3. C. Von Kerckzek, S. Davis, J. Fluid Mech. **62**, 753 (1974)
4. A.V. Coaward, D.T. Papageorgiou, IMA J. Appl. Math. **53**, 75 (1994)
5. M.R. King, D.T. Leighton, M.J. McCready, Physics of fluids **4**, 833 (1999)
6. A.V. Coward, Y.Y. Renardy, J. Fluid Mech. **334**, 87 (1997)
7. V.V. Ramanan, K.A. Kumar, M.D. Graham, J. Fluid Mech. **379**, 255 (1999)
8. C. Davies, P.W. Carpenter, J. Fluid Mech. **352**, 205 (1997)
9. P.G. LaRose, J.B. Grotberg, J. Fluid Mech. **331**, 37 (1997)
10. P.W. Carpenter, P.J. Morris, J. Fluid Mech. **218**, 171 (1990)
11. P.W. Carpenter, A.D. Garrad, J. Fluid Mech. **155**, 465 (1985)
12. P.W. Carpenter, A.D. Garrad, J. Fluid Mech. **170**, 199 (1986)
13. T.B. Benjamin, J. Fluid Mech. **9**, 513 (1960)
14. P.G. Drazin, W.H. Reid, *Hydrodynamic Stability*, (Cambridge University Press, Cambridge, 1981)
15. T.B. Benjamin, J. Fluid Mech. **16**, 436 (1963)
16. M.T. Landahl, J. Fluid Mech. **13**, 609 (1962)
17. V. Kumaran, J. Fluid Mech. **294**, 259 (1995)
18. V. Kumaran, J. Fluid Mech. **302**, 117 (1995)
19. V. Kumaran, J. Fluid Mech. **357**, 123 (1998)
20. V. Kumaran, J. Fluid Mech. **362**, 1 (1998)
21. V. Kumaran, R. Muralikrishnan, Phys. Rev. Lett. **84**, 3310 (2000)
22. R. Muralikrishnan, V. Kumaran, Phys. Fluids **14**, 775 (2002)
23. S.H. Davis, Ann. Rev. Fluid Mech. **294**, 57 (1976)
24. R.M. Thaokar, V. Shankar, V. Kumaran, Eur. Phys. J. B **23**, 533 (2001)
25. V. Shankar, V. Kumaran, Eur. Phys. J. B **19**, 607 (2001)
26. L. Srivatsan, V. Kumaran, J. Phys. II. France **7**, 947 (1997)
27. D.R. Gardner, S.A. Trogden, R.W. Douglass, J. Comput. Phys. **80** 137 (1989)
28. S.A. Orszag, J. Fluid Mech. **50**, 689 (1971)
29. V. Shankar, V. Kumaran, Phys. Fluids **14**, 2324 (2002)